metals

MDPI

Article

Multi-Scale Simulation of Recrystallization during Rolling of Large 2219 Aluminum Alloy Rings

Fengyang He [1,2], Xu Ma [1,2,3,*], Ke Ma [1,3], Yanhong Ding [2,3], Guoming Shi [4] and Chengwu Wang [4]

[1] School of Materials Science and Engineering, Tianjin University of Technology, Tianjin 300384, China
[2] Tianjin Engineering Center of Near-Net-Shape Forming Technology for Metallic Materials, Tianjin 300384, China
[3] Tianjin Key Laboratory of Fastening Technology, Tianjin 300300, China
[4] Tianjin Special Steel Precise Forging Co., Ltd., Tianjin 300302, China
* Correspondence: maxumax@163.com

Abstract: 2219 aluminum–copper alloy is a major material in launch vehicles transition rings. The study of dynamic recrystallization during its rolling and forming process is beneficial to improving the performance enhancement of 2219 aluminum alloy ring parts. In this paper, a multi-scale simulation of grain refinement and distribution of dynamic recrystallization (DRX) grains during the rolling of 2219 aluminum alloy rings is carried out using the finite element method and cellular automata method. On the basis of the JMK DRX model, an ABAQUS subroutine was written to simulate the ring-rolling of 2219 aluminum alloy, and the distribution of DRX percentage and average grain size was analysed from a macroscopic point of view, with a maximum DRX level of 12% and an average grain size distribution from 247 μm to 235 μm from the inside of the aluminum alloy ring towards the surface. A cellular automaton model of DRX during rolling of large aluminum alloys was developed to effectively simulate DRX nucleation, growth, and grain compression deformation during rolling. The DRX nucleation occurs at the grain boundaries and then grows, resulting in a homogeneous organisation and a refinement of grain size, with both the original and DRX grains being compressively deformed as the rolling process progresses and the grains being gradually elongated tangentially. Finally, a comparison of the experimental results with the simulations to obtain grain size and morphology demonstrates consistent results, indicating that the combination of FE and CA methods is an effective approach for a more comprehensive understanding of the microstructural evolution during rolling.

Keywords: large 2219 aluminum alloy rings; CA; dynamic recrystallization; FEM

check for updates

Citation: He, F.; Ma, X.; Ma, K.; Ding, Y.; Shi, G.; Wang, C. Multi-Scale Simulation of Recrystallization during Rolling of Large 2219 Aluminum Alloy Rings. *Metals* **2023**, *13*, 448. https://doi.org/10.3390/met13030448

Academic Editors: Angelo Fernando Padilha and Ramin Hashemi

Received: 10 October 2022
Revised: 29 January 2023
Accepted: 8 February 2023
Published: 21 February 2023

Copyright: © 2023 by the authors. Licensee MDPI, Basel, Switzerland. This article is an open access article distributed under the terms and conditions of the Creative Commons Attribution (CC BY) license (https://creativecommons.org/licenses/by/4.0/).

1. Introduction

Large 2219 aluminum alloy rings are widely used in launch vehicles. The current main processing method for large lightweight ring parts is rolling, which employs ring-rolling equipment to continuously pressurize the ring billet, so that the ring billet continuously passes through the roller, achieving the requirements of diameter enlargement and wall thickness reduction. The warm rolling process results in a significant grain refinement of the ring (a significant reduction in the grain length to diameter ratio) while increasing its strength and plasticity [1] at the same time.

Hua et al. [2] investigated the influence of ring-rolling process parameters on the stiffness conditions of ring parts obtained by establishing a ring stiffness model and conducting finite element simulations. Han et al. [3] analysed the plastic deformation behavior and mechanical properties during the deformation process by numerical simulation of the diameter and axial rolling process of 20CrMnTi alloy. In Ou et al. [4], the microstructure model of AISI 5140 steel was combined with the finite element model of ring rolling to investigate the law of influence of process parameters, such as driver roller speed, core

roller feed rate, and initial temperature of ring billet on the recrystallization behavior of ring parts.

The excellent properties of 2219 aluminum alloy depend on its microstructure. Cellular Automata (CA) models can predict DRX fraction, macroscopic flow pressure, and microstructural evolution, and they have been widely used for various metals and alloys, such as T2 copper [5], 7085 aluminum alloy [6], Ti-55 alloy [7], pure copper [8], NiTi alloy [9], and Hy-100 steel [10]. To accurately model the change in material volume during deformation and its effect on the microstructure through the CA method, the change in topology needs to be considered. Chen et al. [11,12] proposed an updated topological deformation model by developing a cellular coordinate system and a material coordinate system, respectively. The material coordinate system remains unchanged, but the cellular coordinate system and the corresponding particle coordinate system boundary morphology change with the deformation process. Chen et al. [13] extended the conventional CA model to describe the effect of initial grain size on DRX behavior. Sitko et al. [14] proposed a series of improvements on the basis of the basic information assumed in the CA model, such as different dislocation generation schemes, the concept of multiple spaces, and the nuclear size scale, to establish a robust numerical CA model.

On the basis of the data obtained from the hot compression test, a medium temperature numerical model based on the JMK DRX model and a recrystallization model of 2219 aluminum alloy were developed, and a finite element model of ring rolling was built in ABAQUS to study the changes of microstructure during ring rolling of 2219 aluminum alloy at the macroscopic scale. The data obtained from hot compression test and FE model were imported into the established CA model to study the dynamic recrystallization of aluminum alloy at the microscopic scale. Through multi-scale simulations, the recrystallization process of 2219 aluminum alloy during the rolling process was investigated.

2. Materials and Methods

The material used in this study is 2219 aluminum alloy, the chemical composition of which is shown in Table 1. It is made from a blank with an initial outer diameter, inner diameter, and height of 3320 mm, 2500 mm, and 475 mm, respectively. The blank is then rolled on a ringing equipment to form a large aluminum alloy ring with an outer diameter of 6000 mm, inner diameter of 5540 mm, and a height of 425 mm.

Table 1. Chemical composition of 2219 aluminum alloy (wt, %).

Al	Cu	Mn	Ti	Zr	V
Bal.	5.83	0.24	0.055	0.12	0.076

The 2219 aluminum alloy ring selected for this experiment is rolled at 440 °C. In the ring rolling process, as shown in Figure 1, the driver roller provides the driving force for rotation, and the entire ring rolling system rotates through the friction between the ring part and the rollers, while the core roller moves radially at a certain speed, The relationship between time and speed of core roller is depicted in Figure 2, providing the rolling force in the radial direction together with the driver roller, so that the ring part achieves wall thickness reduction. The two conical rollers provide the rolling force in the axial direction to achieve the axial height reduction of the ring. The driver roller, core roller, and conical roller act together on the ring to achieve wall thickness, height deformation, and diameter enlargement of the ring. The process parameters of aluminum alloy rolling are shown in Table 2.

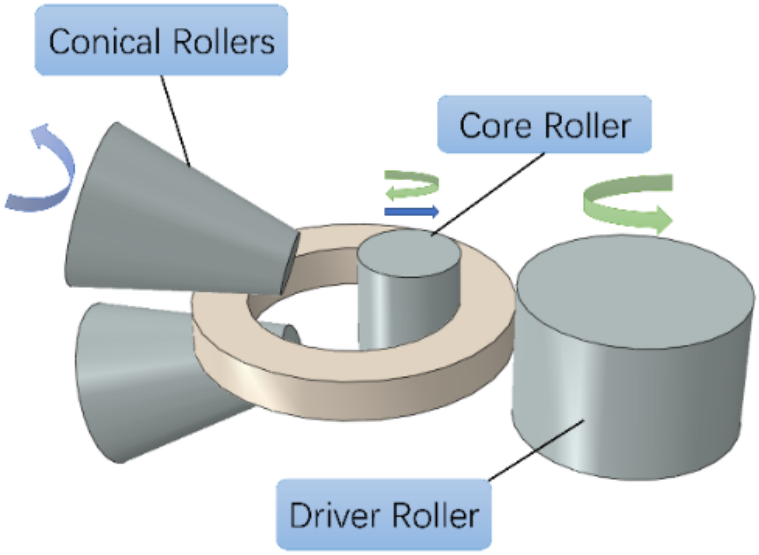


Figure 1. Rolling ring model.

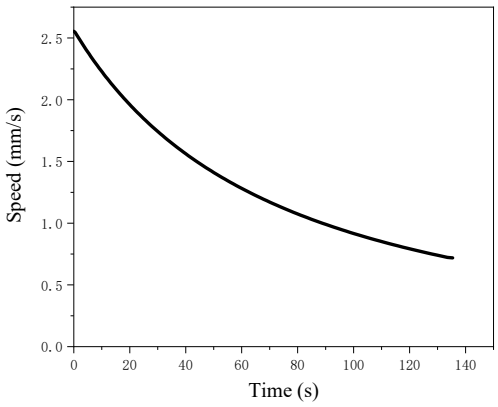


Figure 2. Time vs. speed of core roller.

Table 2. Process parameters of 2219 aluminum alloy.

Driver Roller Size	Core Roller Size	Conical Roller Size	Rolling Temperature	Driver Roller Speed
1350 × 1700	600 × 1700	402 × 80.4 × 30	440 °C	1.5 rad/s

Sample preparation is prepared by cutting the sample after rolling processing by Wire Electrical Discharge Machining (EDM), and the position of the sample is shown in Figure 3; the metallographic samples, with an initial size of approximately 8 mm × 8 mm × 5 mm, were inlaid, ground, and mechanically polished. During the polishing process, ordinary 180-, 600-, 1000-, and 2000-Cw sandpapers were first used, after which 1200# and 2000# metallographic sandpapers were used, and, finally, W1.0 and W0 polishing pastes were employed. They were then chemically corroded with Keller's reagent, and the metallographic structures were observed using an Olympus DSX500 metallographic microscope.

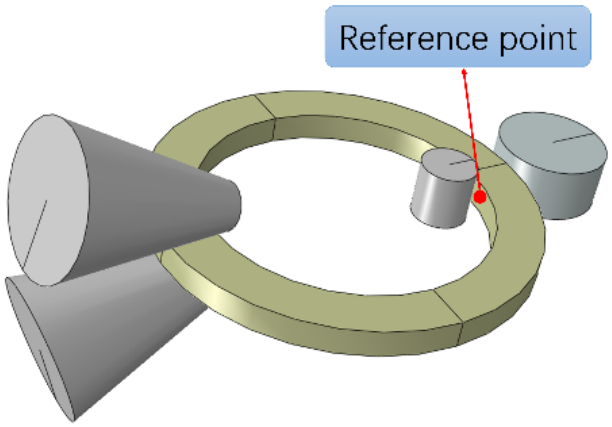


Figure 3. Reference point position of the sample.

3. Simulation Process

3.1. Finite Element Simulation

In the rolling process, plastic deformation and temperature increases will cause microstructure changes, especially in the serious areas of plastic deformation, which will lead to grain refinement and dynamic recrystallization by thermal activation. As the rolling process proceeds, plastic deformation, strain rate, and temperature increase, and changes, such as a remarkable reduction in the time of heat transfer, have a significant impact on the evolution of the microstructure. A modified JMAK DRX model was implemented in a VUHARD Fortran subroutine to predict the grain size distribution in rolling metals using ABAQUS/Explicit FEA software. This model is represented by Equations (1)–(8).

In this paper, the Arrhenius equation proposed by Sellars and McTrgart is used to describe the effect of deformation temperature and strain rate on the variation of flow stress levels during hot forming of 2219 aluminum alloy [15].

$$\dot{\varepsilon} = A[sinh(\alpha\sigma)]^n exp(-Q/RT) \tag{1}$$

where $\dot{\varepsilon}$ is the strain rate (s^{-1}), R is the universal gas constant (8.31 J mol^{-1} K^{-1}), T is the absolute temperature (K), Q is the activation energy of hot forming (kJ mol^{-1}), and A, α, and n are the material constants.

Due to the complexity of dynamic recrystallization and high temperature deformation in hot compression tests, the dynamic recrystallization behavior is generally characterized by three stages: initial, acceleration, and stabilization, and is characterized by an "S" shape [16]. Among the many classical DRX kinetic models, Avrami's equation can accurately describe the kinetic process of recrystallization and, therefore, is widely used.

$$X_{drex} = 1 - \exp\left[-\beta_d\left(\frac{\varepsilon - \varepsilon_c}{\varepsilon_{0.5}}\right)^{k_d}\right] \tag{2}$$

where β_d and k_d are the material constants, and $\varepsilon_{0.5}$ is the strain value at a DRX volume fraction of 0.5, which can be expressed as

$$\varepsilon_{0.5} = a_1 Z^{m_1} \tag{3}$$

where a_1 and m_1 are the material constants.

In general, the critical strain at which DRX occurs, ε_c, and the peak strain, ε_p, are approximately linear; thus, it is necessary to investigate and establish the relationship of ε_p with the Z parameter. The following equation was obtained by linear regression.

$$\varepsilon_c = a_2 Z^{m_2} \tag{4}$$

$$\varepsilon_c = a_3 \varepsilon_p \tag{5}$$

where Z, the Zener–Hollomon parameter, is a characteristic parameter regarding the strain rate as well as the deformation temperature.

$$Z = \dot{\varepsilon} exp\left(\frac{Q}{RT}\right) \tag{6}$$

Dynamic recrystallization grain size refers to the size of the grain when the recrystallization process of metals and alloys reaches a steady state where the dynamic recrystallization grain size d_{drex} remains essentially constant as the strain increases.

$$d_{drex} = a_4 Z^{m_3} \tag{7}$$

The average grain size is the average value of the remaining original grain size and new formed DRX grain size, which can be calculated by:

$$= d_0(1 - X_{drex}) + d_{drex} X_{drex} \tag{8}$$

To obtain the parameters in the above model, the experimental data were processed accordingly, and the following JMAK DRX model was obtained.

$$\begin{cases} \dot{\varepsilon} = 2.457E9[sinh(0.02283\sigma)]^{6.47674} exp(-141178.1/RT) \\ \varepsilon_c = 0.4766\varepsilon_p \\ \varepsilon_c = 0.00775Z^{0.12376} \\ X_{drex} = 1 - \exp\left[-0.5962\left(\frac{\varepsilon - \varepsilon_c}{\varepsilon_{0.5}}\right)^{1.41386}\right] \\ \varepsilon_{0.5} = 0.00337Z^{0.22012} \\ d_{drex} = 96.73762Z^{-0.07605} \\ d = d_0(1 - X_{drex}) + d_{drex} X_{drex} \end{cases}$$

To predict the DRX kinetics and grain size, Xu [17] developed a user subroutine VUHARD in FORTRAN by using the JMAK model. The ring–rolling process was modeled in the finite element software ABAQUS. The 2219 modified JMAK DRX model was then imported and set as the ring material parameter, and the average grain size and initial grain size of each mesh of the ring were set to 300 μm. The shape of the aluminum ring before and after the rolling simulation is shown in Figure 4.

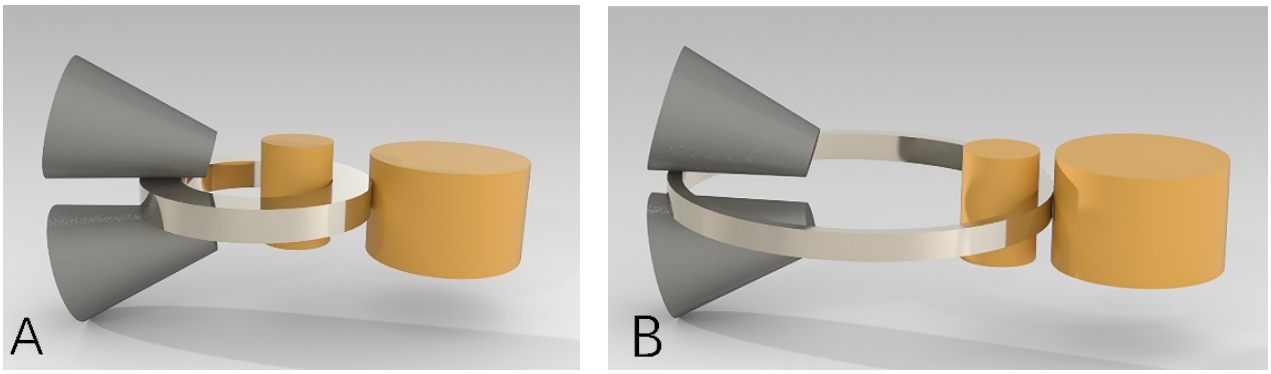


Figure 4. Schematic diagram of the rolling model: (**A**) before rolling and (**B**) after rolling.

3.2. Cellular Automata Simulation

Cellular automata is a time-discrete, spatially discrete mathematical model that describes various complex system states through transformation rules between cells.

3.2.1. Dislocation Density Evolution Model

The process of plastic deformation of metals is accompanied by a change in dislocations. To describe the dislocation density evolution of 2219 aluminum alloy during plastic deformation, the KM (Kocks–Mecking) [18] model has been employed for modeling, in which the flow stress (σ) is proportional to the square root of dislocation density (ρ), as given in Equation (9).

$$\sigma = \alpha \mu b \sqrt{\overline{\rho}} \tag{9}$$

where α is a constant, depending on the Poisson's ratio, and the dislocation arrangement, orientation, and other microstructure states, usually called the dislocation interaction coefficients, are generally taken as 0.5 for metals. $\overline{\rho}$ is the mean dislocation density; b is the Burgers vector; and μ is the shear modulus. In the simulation, the average dislocation density can be obtained by the following equation.

$$\overline{\rho} = \frac{1}{N} \sum_{ij} \rho_{ij} \tag{10}$$

where N is the total number of the cells in the CA simulation, and ρ_{ij} is the dislocation density of cells with site (i,j). During the thermal deformation process, the dislocation hardening resulting from the deformation leads to the dislocation density multiplication, and the softening resulting from the recovery and dynamic recrystallization leads to the annihilation of dislocation density. The effect of work-hardening and -softening on the change in dislocation density is considered according to the KM model. The model considers the relationship between dislocation density ρ and strain ε as

$$\frac{d\rho_{ij}}{d\varepsilon} = k_1 \sqrt{\rho_{ij}} - k_2 \rho_{ij} \tag{11}$$

where the first term represents the effect of process hardening on dislocation density, and the second represents the effect of dynamic softening on dislocation density. k_1 and k_2 can be obtained from the following equation.

$$k_1 = \frac{2\theta_0}{\alpha \mu b} \tag{12}$$

$$k_2 = \frac{2\theta_0}{\sigma_s} \tag{13}$$

where θ_s is the saturation stress, and θ_0 is the hardening rate, which can be obtained from the slope of the work-hardening phase in the stress–strain curve.

3.2.2. Model of Nucleation and Growth

Dynamic recrystallization nucleation is usually associated with the accumulation of dislocations. When the dislocation density of a deforming matrix reaches a critical value (ρ_c) during thermos–mechanical processing, nucleation of DRX will be initiated. In the simulations, nucleation is assumed to occur at the initial grain boundaries with sufficient stored energy, which accumulates to a certain level before the initial grain boundary nucleation takes place. The dislocation density of the recrystallized grains is close to zero, and the grain orientation is represented by a random integer in the range of 1–180. In a previous study, Ding and Guo showed that the recrystallization nucleation rate exists as a function of temperature and strain rate, and they proposed the following nucleation rate model [19].

$$\dot{n}\left(\dot{\varepsilon}, T\right) = C\dot{\varepsilon}^m exp\left(-\frac{Q_{act}}{RT}\right) \tag{14}$$

where C is a material constant, m is set to 1 in each s, and Q_{act} is the activation energy.

For the critical dislocation density, ρ_C is calculated, which can be expressed by the following equation:

$$\rho_c = \left(\frac{20\gamma_i\dot{\varepsilon}}{3blM\tau^2}\right)^{1/3} \tag{15}$$

where γ_i is the grain boundary energy, $\bar{\varepsilon}$ is the strain rate, l is the dislocation mean-free path, M is the grain boundary mobility, and τ is the dislocation line energy ($\tau = cub^2$, where c is a constant equal to 0.5). The interfacial energy can be expressed according to the Read–Shockly equation as

$$\gamma_i = \begin{cases} \gamma_m & \theta_i \geq 15^\circ \\ \gamma_i = \gamma_m \frac{\theta_i}{\theta_m}\left(1 - ln\left(\frac{\theta_i}{\theta_m}\right)\right) & \theta_i < 15^\circ \end{cases} \tag{16}$$

where θ_i is misorientation between the ith DRX grain and the neighboring grains, and θ_m and γ_m are the misorientation and grain boundary energies (assumed to be 15°) for large-angle grain boundaries, respectively, where the grain boundary energy γ_m can be obtained from the following equation:

$$\gamma_m = \frac{\mu b\theta_m}{4\pi(1-v)} \tag{17}$$

where ν is Poisson's ratio. After dynamic recrystallization, the difference between the dislocation densities of DRX grain and the matrix supplies the thermodynamic driving force for the growth of DRX grain. The growth rate of recrystallized grain i, v_i, satisfies the following relationship with the driving force acting on its unit area:

$$v_i = \frac{MF_i}{4\pi r^2} \tag{18}$$

where M is the grain boundary mobility, and it is given by [20]:

$$M = \frac{\delta D_{ob} b}{KT} exp\left(-\frac{Q_b}{RT}\right) \tag{19}$$

where δ is the characteristic grain boundary thickness, D_{ob} is the boundary self-diffusion coefficient, Q_b is the grain boundary diffusion activation energy, and K is the Boltzmann constant.

Grain growth is driven by the reduction of stored energy. For dynamic recrystallization, in addition to the grain boundary energy in the system, the distortion energy due to deformation has an important influence on the growth of recrystallized grains. Assuming spherical grains, the driving force F_i can be calculated from the energy change (dw) of the DRX grain growth process. For each DRX grain with radius of r growth, the energy change is given by the volume energy dW_{vol} and surface energy dW_{sur}, which can be expressed by the following equation:

$$dW = dW_{vol} + dW_{sur} \tag{20}$$

$$dW_{vol} = \tau\left(\frac{4}{3}\pi(r+dr)^3 - \frac{4}{3}\pi r^3\right)(\rho_d - \rho_m) = 4\pi r^2\tau(\rho_d - \rho_m)dr \tag{21}$$

$$dW_{sur} = d\left(4\pi r^2\gamma\right) = 8\pi r\gamma dr \tag{22}$$

Therefore, the driving force F_i can be found by the following equation:

$$F_i = -\frac{dW}{dr} = 4\pi r_i^2\tau(\rho_m - \rho_i) - 8\pi r_i\gamma_i \tag{23}$$

where ρ_i is the dislocation density of the ith DRX grains, and ρ_m is the dislocation density of the parent grain. Let $\Delta\rho = \rho_m - \rho_i$; then, dividing the driving force by the boundary area of the spherical grain, we can obtain the driving force acting on the boundary:

$$f_i = \tau\Delta\rho - 2\gamma_i/r_i \tag{24}$$

3.2.3. Topological Deformation Techniques

During deformation, grains are compressed along the compression direction and elongated along the vertical direction. Deformation directly changes grain morphology, grain surface area per unit volume, and grain boundary length, and it further affects the DRX process of the material. The effect of deformation on grain topology is, therefore, another issue to be considered in DRX-CA simulations. Typical two-dimensional CA models are usually based on periodic square cells, where parallel sides can be defined as vectors, such that rectangular cells can be described by only two vectors (0,1) and (1,0). Adjacent cells with the same orientation are considered to be the same grain, while adjacent cells with different orientations are separated by grain boundaries. Thus, the deformation of grain can be transformed into the deformed square unit cell inside the grain. The transformation process can be expressed by the following equation:

$$\begin{pmatrix} v_1 \\ v_2 \end{pmatrix} = \begin{pmatrix} S_{11} & S_{12} \\ S_{21} & S_{22} \end{pmatrix} \begin{pmatrix} u_1 \\ u_2 \end{pmatrix} \tag{25}$$

where u is the original vector, and v is the new vector after each DRX cellular automata step. The elements s_{ij} of the deformation matrix S are determined by the type of deformation. In the plane strain issue, all cells are zero except for the diagonal cells S_{11} and S_{22}. (S_{11} and S_{22} are the ratios of the final to the initial lengths of the vectors of the main nominal deformations in both directions along the two principal axes). Thus, $\varepsilon_{11} = ln\, s_{11}$ and $\varepsilon_{22} = ln\, s_{22}$ are the true strains along the main axis direction of deformation. Since the volume remains constant during the deformation, the determinant of S must be in units ($S_{11}S_{22} = 1$)

In the CA simulation, each cell is treated as a discrete point in space, and the geometric changes in each cell at each deformation step are calculated by employing a topological deformation model. The same deformation is applied to all cells; therefore, the model can track the changes in the morphology of each grain during the deformation process. On the basis of the above approach, a CA model that considers the topological deformation of the grains is developed to relate the material microstructural evolution to the deformation parameters. Therefore, the simulation results are of practical significance.

3.2.4. Initial Setup of Cellular Automata and FEM

On the basis of the above dynamic crystallization theory, the corresponding program was coded in Matlab in conjunction with the principle of the cellular automaton. In this study, because CA simulation of microstructure evolution is conducted with the increase in strain—in which time step is $\Delta t = \varepsilon/\left(N\dot{\varepsilon}\right)$, where N is the total iteration step, and 700 steps are adopted, and the data from the finite element simulation and experiment were imported into the cellular automaton—the initial average grain size is 300 μm, which was obtained from OM on an unprocessed sample (as Figure 5), the size of the simulation is 750 × 750 cell space, and each cell size represents 4 μm of the actual grain size. Therefore, the actual material range of the simulation is 3 mm × 3 mm, and the initial grain microstructure model is shown in Figure 6. The ring parts are divided into 34,048 elements with type C3DRT, the remaining parts are set up as rigid body with element type R3D4, and the processing temperature is 440 °C. The driver roller and core roller rotate around the central axis at a speed of 1.5 rad/s, while the core rolls can move towards the driver roller at the same time. The upper conical roller can rotate on its own central axis while moving downwards in the Z direction. The flowchart [17] of the calculating process of user subroutine VUHARD is

shown in Figure 7, and the flowchart of the data combined with the cellular automaton is shown in Figure 8.

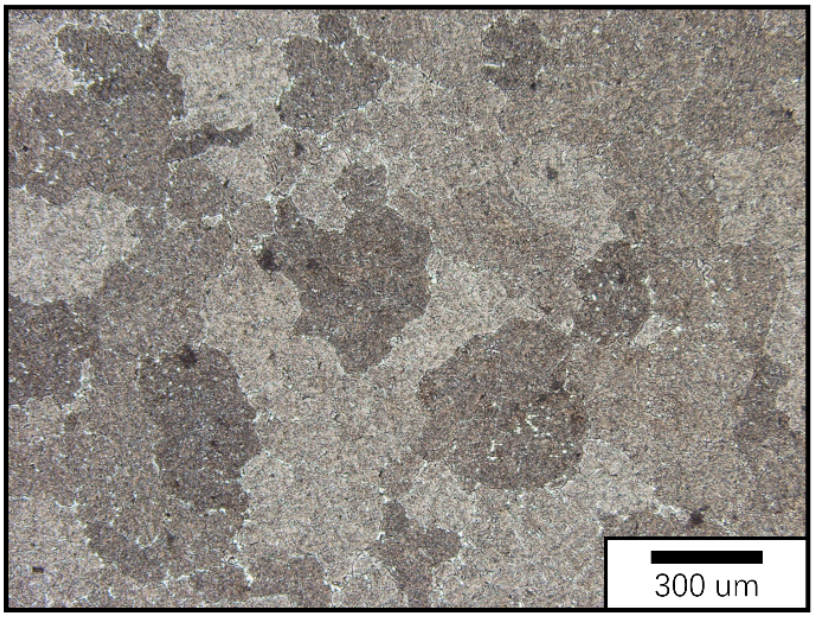


Figure 5. Initial grain morphology.

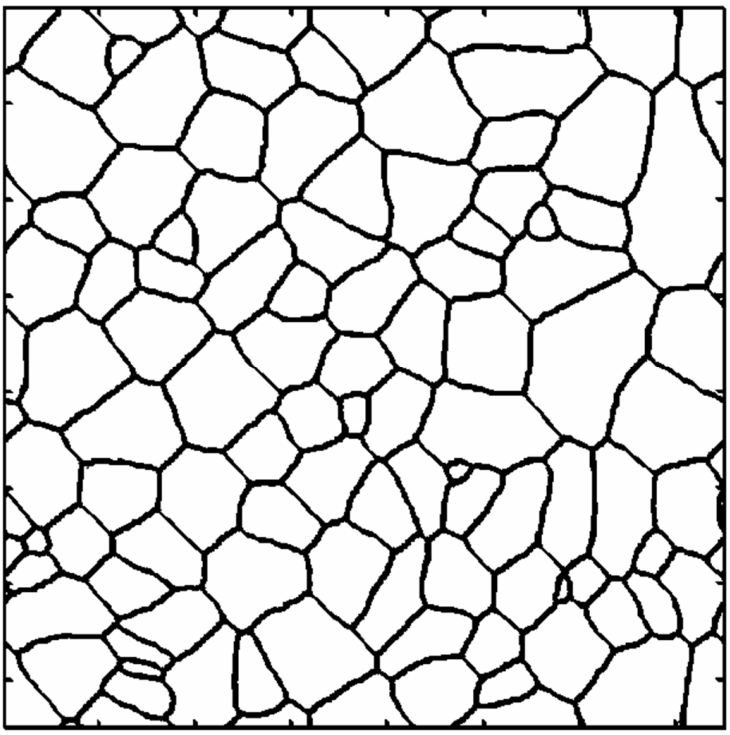


Figure 6. Initial grain model.

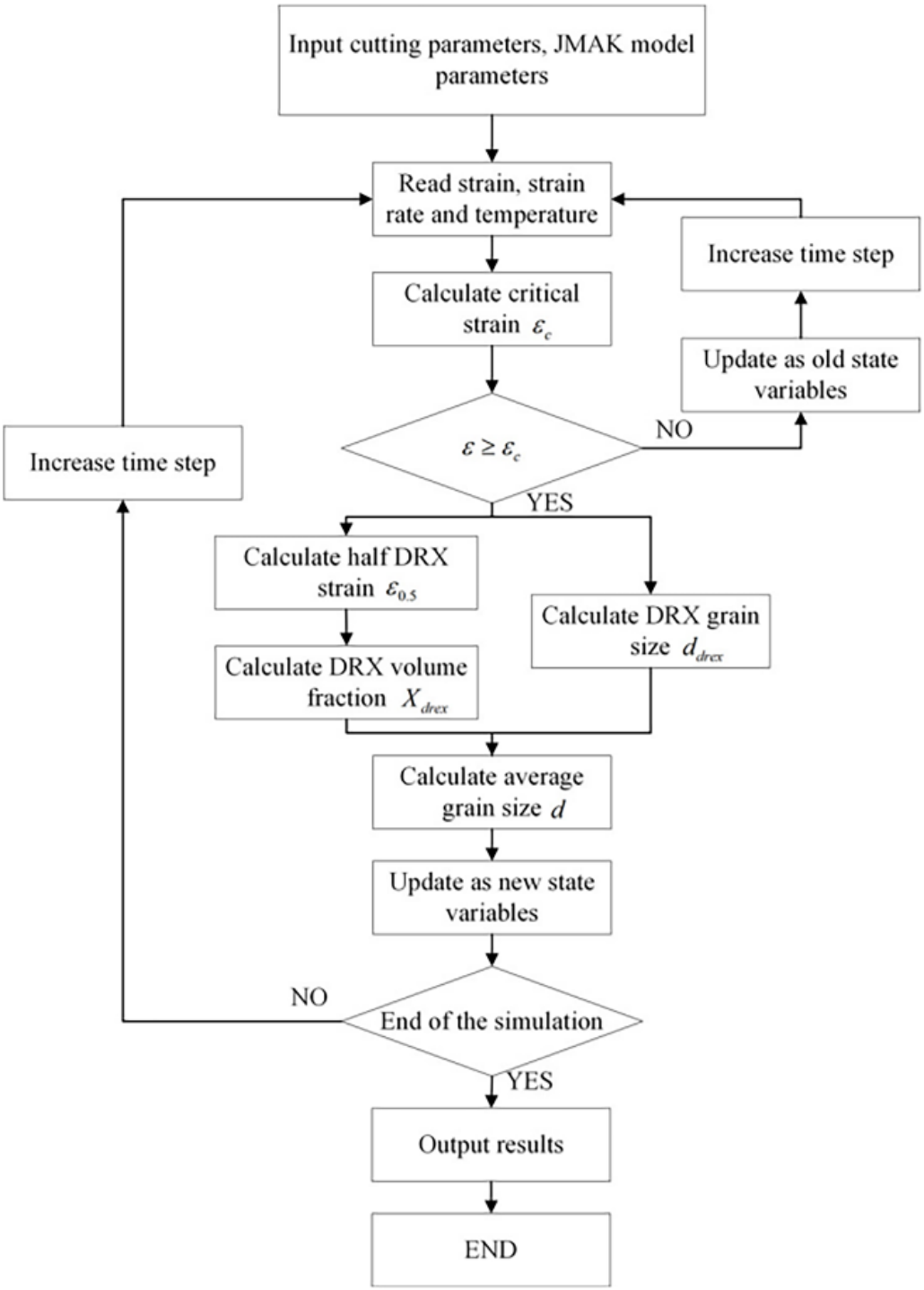


Figure 7. Flowchart of subroutine VUHARD using JMAK model.

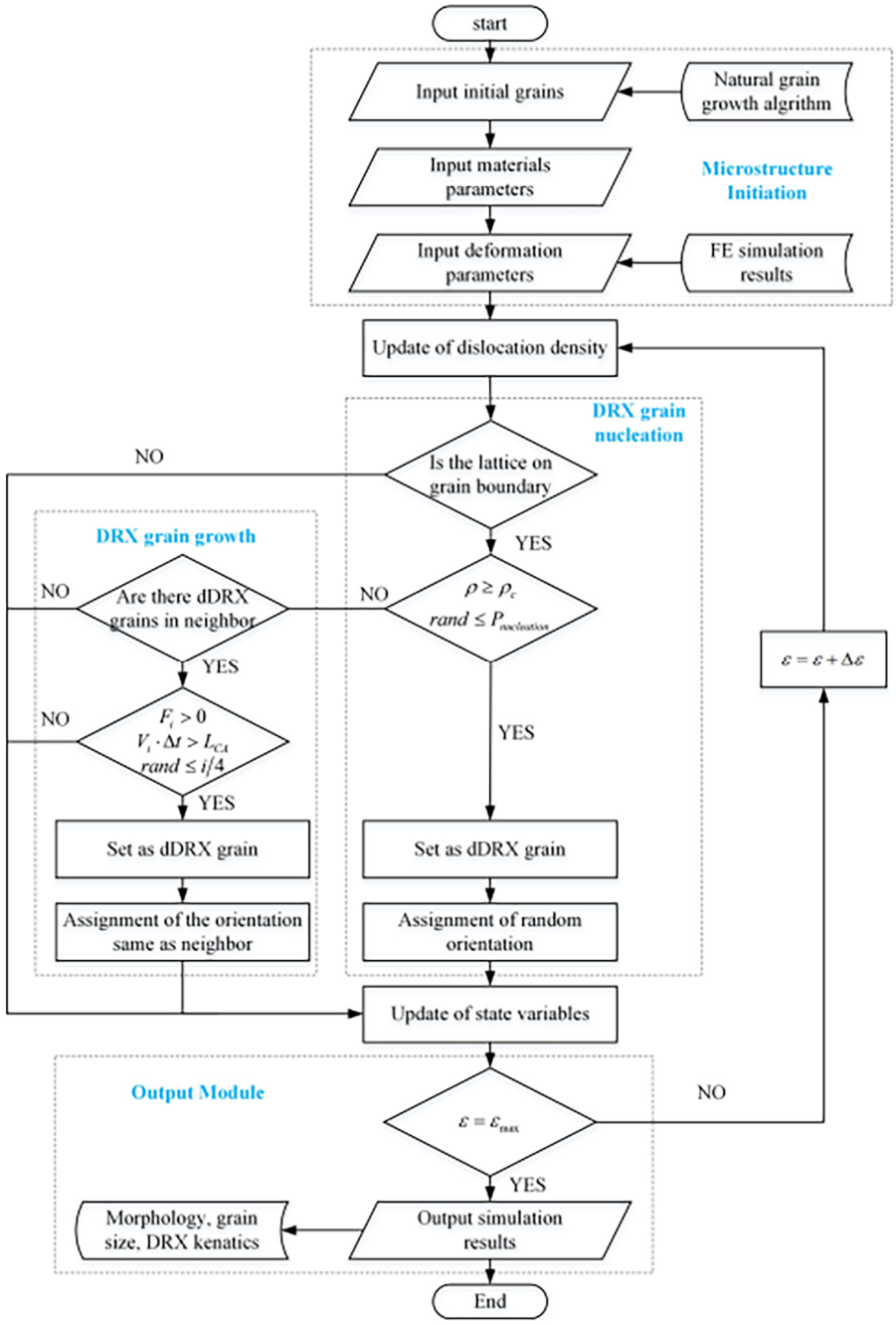


Figure 8. Flowchart of CA simulation.

4. Analysis of Results

4.1. Evaluation of the FE Models

To verify the computational results, the FE model was compared with the experimental results to determine the relative error, and the outer diametrical growth rate for both the simulation and experiment were compared, revealing a maximum relative error of 4% in growth, as seen in Figure 9. Upon comparison with the experiments, the accuracy of the simulation can be verified. The errors can be attributed to the measurement process and material properties.

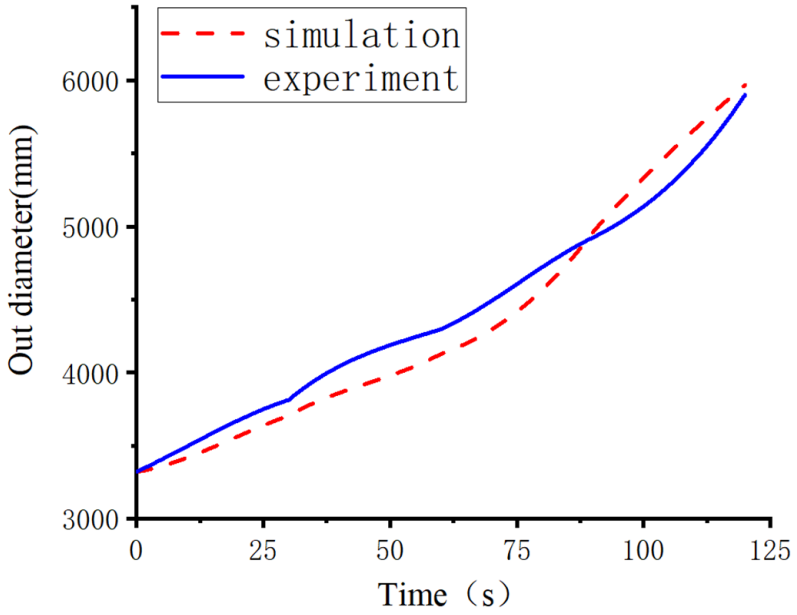


Figure 9. Outer diameter growth rate for simulation and experiment.

4.2. Distribution of Recrystallization Percentages

In the entire ring-tying process, due to a large number of rollers, the entire forming process has two forming areas, namely the driver roller and core roller area and the axial rolling area formed by two conical rollers. The entire process is divided into four analysis stages: (1) driver roller bite stage, (2) conical roller bite stage, (3) stable rolling stage, and (4) rolling completion stage. At the beginning of the rolling stage, the first to proceed is the driver roller bite stage, as shown in Figure 10A; due to the radial movement of the core rollers and the drive of the drive rollers, the first dynamic recrystallisation occurs in the area in contact with the core rollers. This is because the deformation in this area causes the dislocation density to increase, after the dynamic recrystallization firstly occurred driven by the temperature and stress conditions. As the rolling process progresses, the deformation zone of the conical rollers also produces DRX, as shown in Figure 10B, where DRX occurs in the contact area because the rolling of the conical rollers in the axial direction increases the energy in the deformed part, thus contributing to the formation of DRX. With the rotation of the workpiece, the initial part of the DRX was due to diffusion, causing the ring to DRX to different degrees, as can be seen in Figure 10C, where the outer surface of the ring has a higher degree of DRX than the inner surface. From Figure 10D, it can be seen that the highest degree of recrystallisation until the completion of the rolling stage is on the outer surface and the intersection of the upper and lower surfaces because in this area, which is the most severely deformed area, the dislocation density changes rapidly, so that the highest percentage of recrystallisation can be achieved, with a maximum dynamic recrystallisation percentage of 53%.

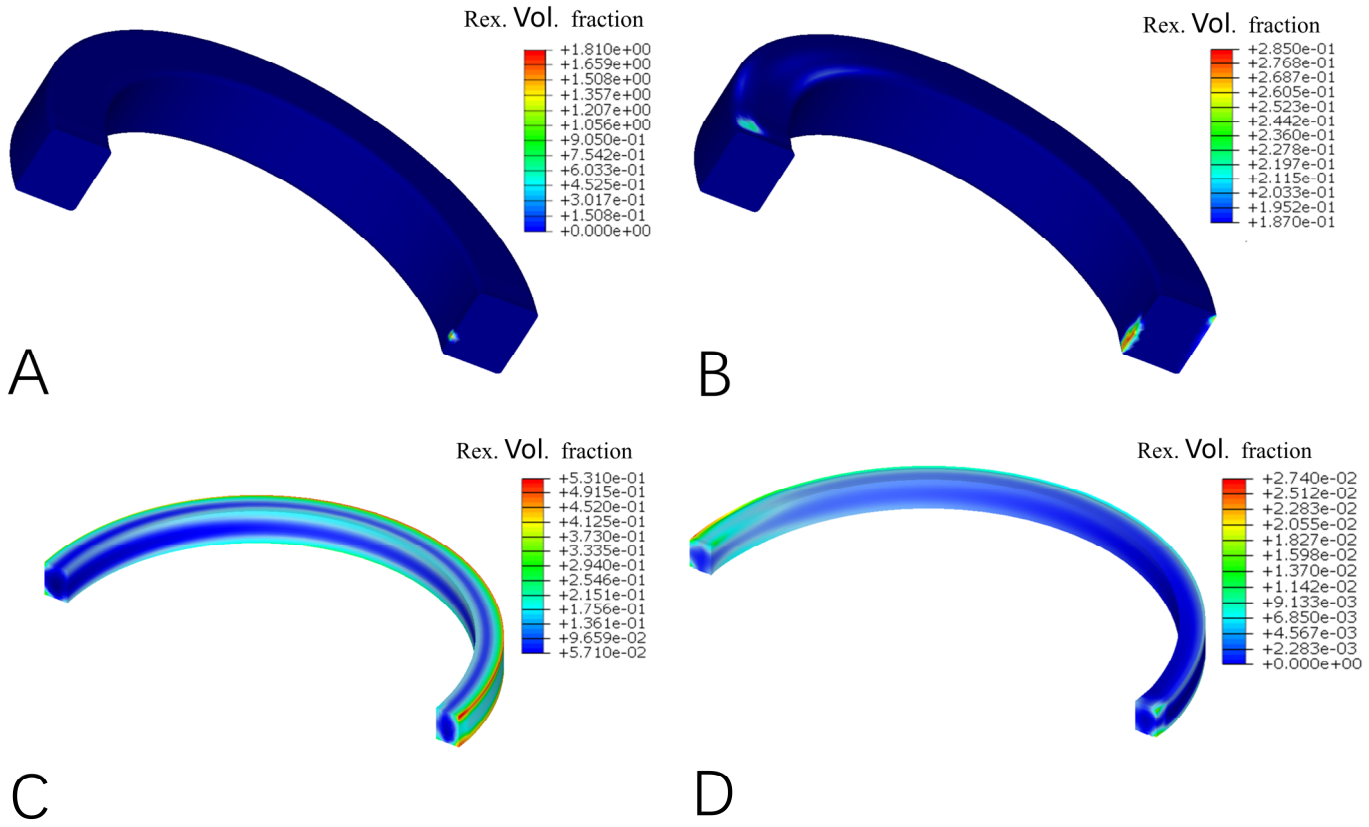


Figure 10. Distribution of DRX percentages of 2219 aluminum alloy during ring lashing: (**A**) Drive roll bite stage, (**B**) Vertebral roll bite stage, (**C**) Stable rolling stage, and (**D**) Rolling completion stage.

4.3. Average Grain Size Distribution

Figure 11 shows the process of grain-scale change in the aluminum alloy ring from two viewpoints, the inner and outer wall parts of the ring. It can be seen from the figure that as the rolling process proceeds, the grain size changes gradually. Figure 11A shows the initial average grain size is set at 300 μm according to experimental observations before the start of rolling. With the movement of the driver roller, the bite stage of the driver roller in Figure 11B—in the deformation zone consisting of the driver roller and the core roller—causes the ring part to be deformed due to pressure and friction. On the one hand, the internal grains are subjected to radial pressure and tangential shear stress, which causes the grains to be deformed, and on the other hand, the deformation causes the dislocation density to be increased, providing the driving force for dynamic recrystallization. Under the combined effect of grain deformation and dynamic recrystallization, the grain scale is reduced, and the grains are refined. As the ring rolling process, the grain scale of the inner part of the aluminum alloy ring begins to decrease. When rolling enters the stable stage, i.e., Figure 11C, the grain size of the inner and outer surface of the aluminum alloy ring is smaller than that of the inner part of the aluminum alloy, the average grain size of the inner part of the alloy is 250 μm, and the smallest average grain size of the outer surface is 150 μm. At the rolling completion stage, i.e., Figure 11D, the grain distribution is still not uniform, and the internal grain size is larger, while the inner and outer wall grain size is smaller, the largest average grain size is 247 μm, and the smallest average size is 235 μm.

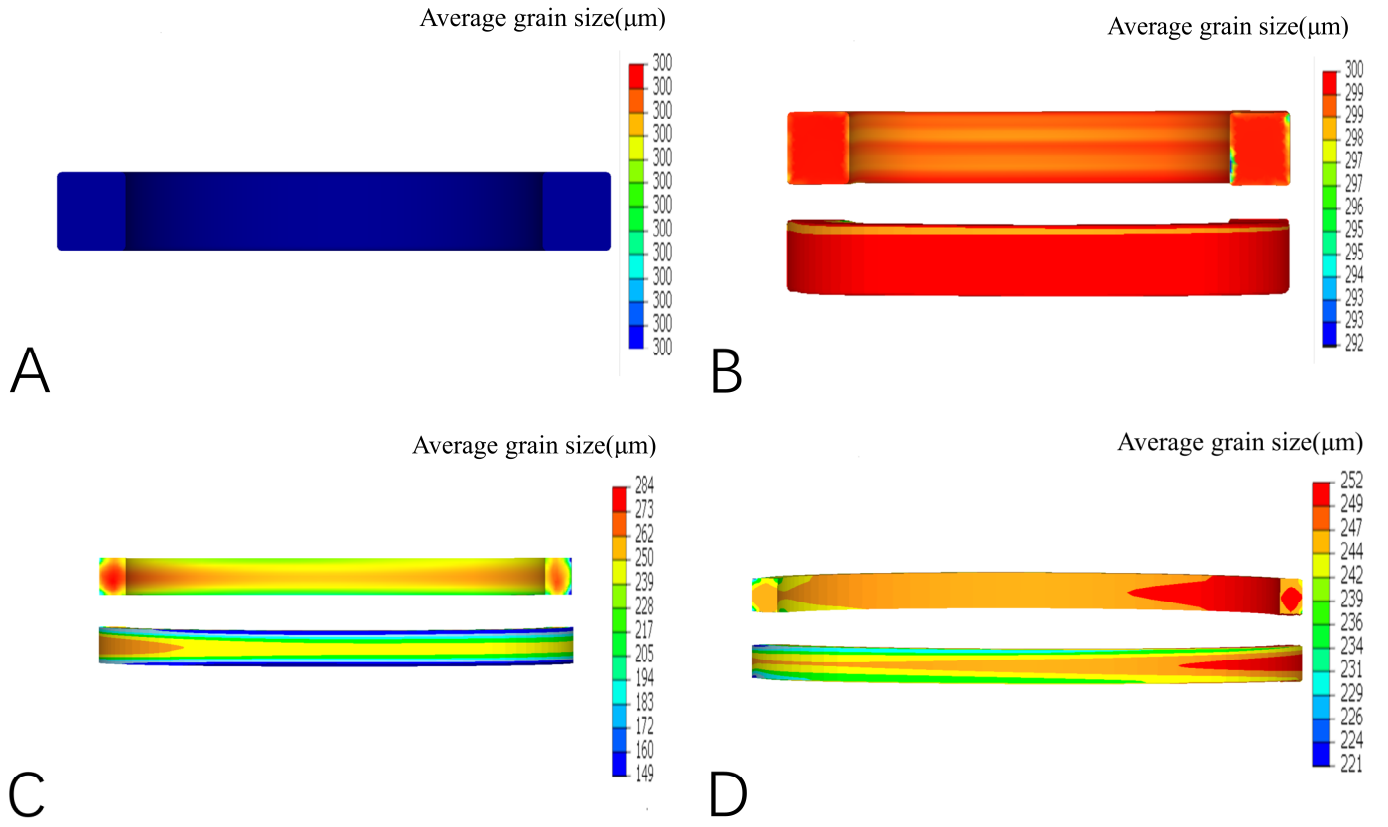


Figure 11. Grain size distribution of 2219 aluminum alloy during ring tying: (**A**) Drive roll bite stage, (**B**) Vertebral roll bite stage, (**C**) Stable rolling stage, and (**D**) Rolling completion stage.

4.4. FEM and CA Multi-Scale Simulations of Dynamic Recrystallized Grain Distribution

Regarding the average grain size distribution that both the FEM and CA methods are able to simulate, the FEM method is better at showing the grain distribution in different areas of the workpiece on a macroscopic scale, while the CA method is better at visualizing the microscopic morphology at a point. The physical process of grain evolution can be reproduced, which helps to investigate the influence of microstructural evolution on the mechanical behavior.

The average grain size distribution of the entire ring-rolled part can be obtained from FEM. For a small area, the grain size distribution can be shown by the results of CA. The implementation of the CA model allows for a direct comparison of test results between the simulation and the experiment, as opposed to a single-rolled finite element simulation of the microstructure evolution. Figure 12 shows that, in the FE model, the distribution of dynamic recrystallization grain size is affected by the process: the larger dynamic recrystallization grains are distributed mainly in the deformation zone consisting of driver roller and core roller, whereas, with the direction of rolling, the smaller DRX grains have not entered the deformation zone. This is because the growth of the recrystallized grains needs to be stress-driven to have enough energy to allow the DRX grains to continue growing. In Figure 12B, it can be seen that the recrystallized grains are located mainly at the grain boundaries of the initial grains and that the recrystallized grain size is smaller than the initial grain size, which results in a decrease in the average grain size and allows the grains to be refined. Therefore, combining the FEM with the CA model provides a more comprehensive and multi-scale method to understand the microstructural evolution of the process and its effect on the aluminum alloy rolling process.

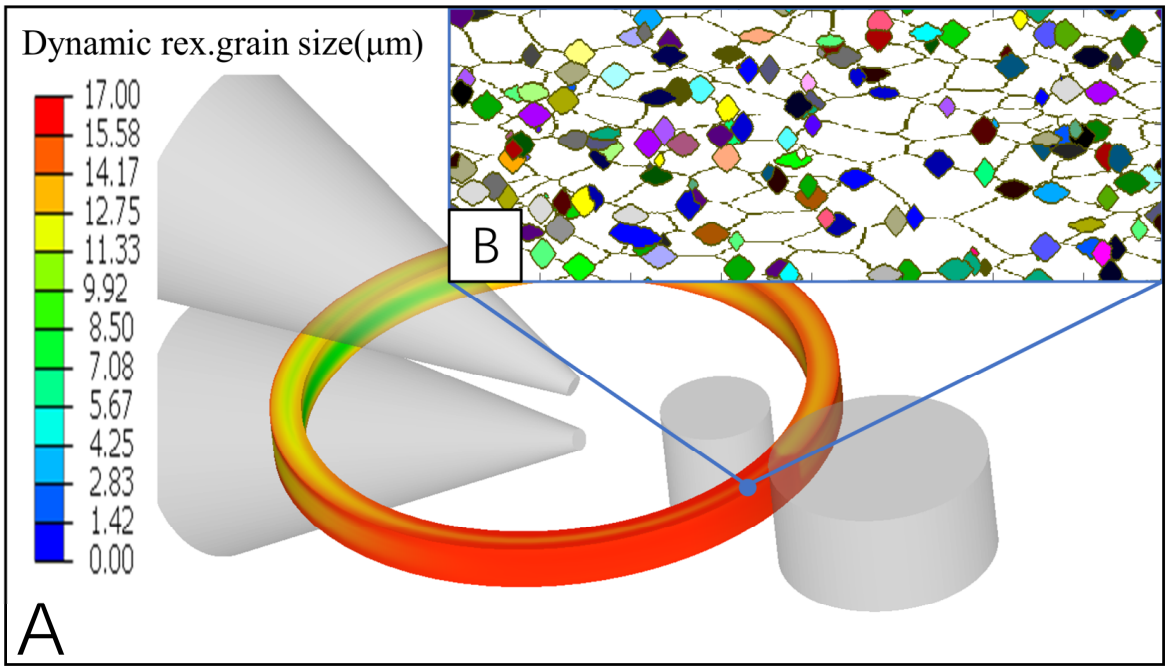


Figure 12. (**A**) Distribution of DRX grain size under FEM (**B**) Distribution of DRX grain size under CA at reference point.

4.5. Grain Refinement Mechanism of 2219 Aluminum Alloy in Ring-Rolling Process

A selected point on the inner wall of the ring member is used as a reference point for the study, and the simulation data from this point are imported into a cellular automata to observe the simulation process of its microstructural transformation. Figure 13 shows the nucleation and recrystallization of the grains during the simulation. At the beginning of the rolling, the grain shape does not change significantly, as the rolling stage proceeds, in the stage of the driver roller and cone roller bite in. When dislocation density increases to critical dislocation density, a new nucleus appears at the grain boundary of the initial grain, as shown in Figure 13A; this stage is called dynamic recrystallization nucleation stage. At the same time, due to the pressure from the rollers, the grain shape is changed and elongated in the tangential direction of the aluminum alloy ring, as shown in Figure 13B. The misorientation and dislocation density between the newly formed grains and the original grains provide the driving force for newly formed grains to grow slowly. After the emergence of new nuclei, the nucleation and growth occur simultaneously, which increases the area of new grains, but the newly formed grains grow more slowly. While the growth process is accompanied by dynamic recrystallization nucleation, making the size of recrystallized grains smaller than the original grain size due to the nucleation and the diffusion of new grains into the original grains during the growth process, they occupy some of the space of the original grains, which reduces the size of the original grains, thus reducing the overall grain size and resulting in overall grain refinement. However, due to the pressure, all the grains are compressed and elongated. The process of grain deformation is shown in Figure 13A–C.

As the rolling process continues, the strain gradually becomes larger. Figure 14 illustrates the relationship between the percentage of dynamic recrystallisation (PODRX) and the strain. It can be seen that when strain accumulates to approximately 0.1, the dynamic recrystallization initiates, and the percentage of dynamic recrystallisation becomes progressively larger as the strain increases.

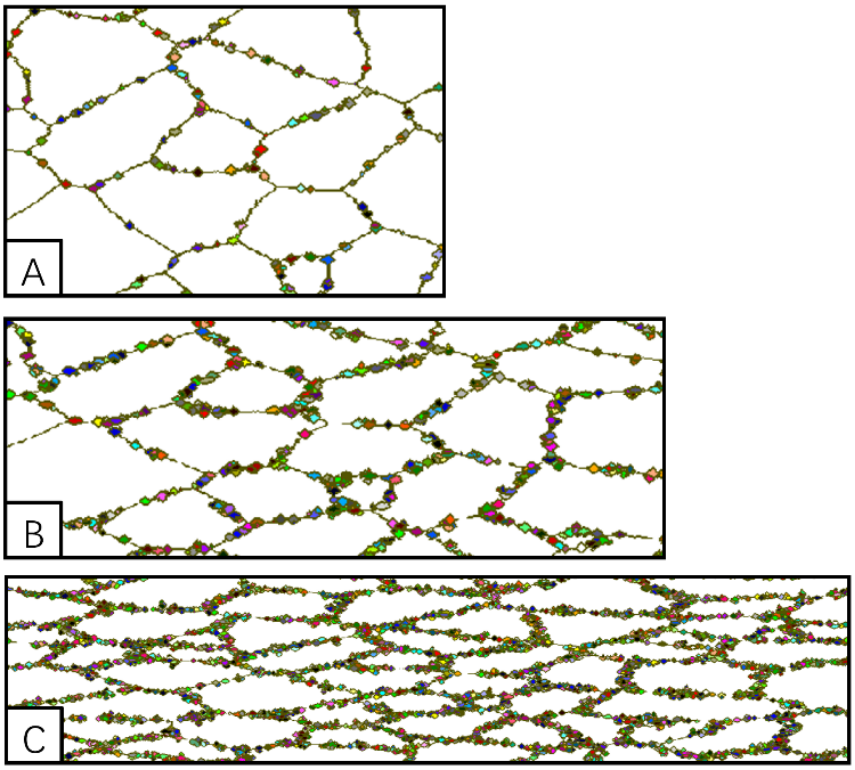


Figure 13. Grain deformation diagram during CA simulation at Different stages (**A**) dynamic recrystallization nucleation initial stage (**B**) grain shape change stage (**C**) final stage.

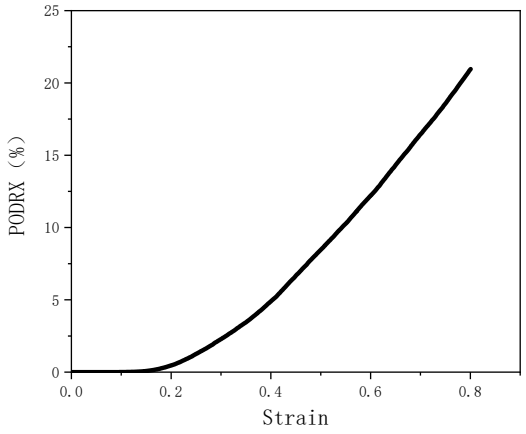


Figure 14. Relationship between PODRX and strain.

The relationship between the mean size of dynamic recrystallized grain (MSODRXG) and strain is given in Figure 15, from which it can be seen that the mean size of dynamic recrystallized grain size increases with strain and becomes progressively larger. However, when the strain is greater than 0.3, there is a strain region in which the mean size of dynamic recrystallized grain size decreases as the strain increases. This is due to the generation of new grain during the dynamic recrystallization process, and as can be seen in Figure 14, after strain greater than 0.3, the percentage of dynamic recrystallisation changes is significantly faster, which means that the rate of nucleation is accelerating. This causes the mean size of dynamic recrystallized grain to decrease in certain strain ranges due to the smaller size of the larger number of newly generated grains.

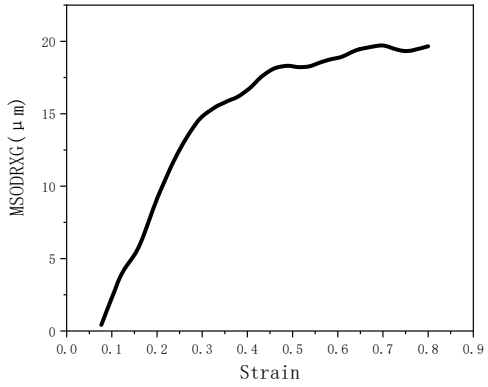


Figure 15. Relationship between MSODRXG and strain.

The microstructure of the rolling results is shown in Figure 16. It can be seen that the simulated results and the experimental microstructure have the same isometric structure and clear rolling direction, and recrystallized grains are formed at the grain boundaries. The results show that as the deformation increases during rolling, the deformation energy in the metal increases, and the grains are elongated along the rolling direction due to the rolling pressure. The grain shape after rolling is consistent with the simulation results, while the position distribution of the recrystallized grains is consistent with the simulation results, which verifies the validity of the simulation process.

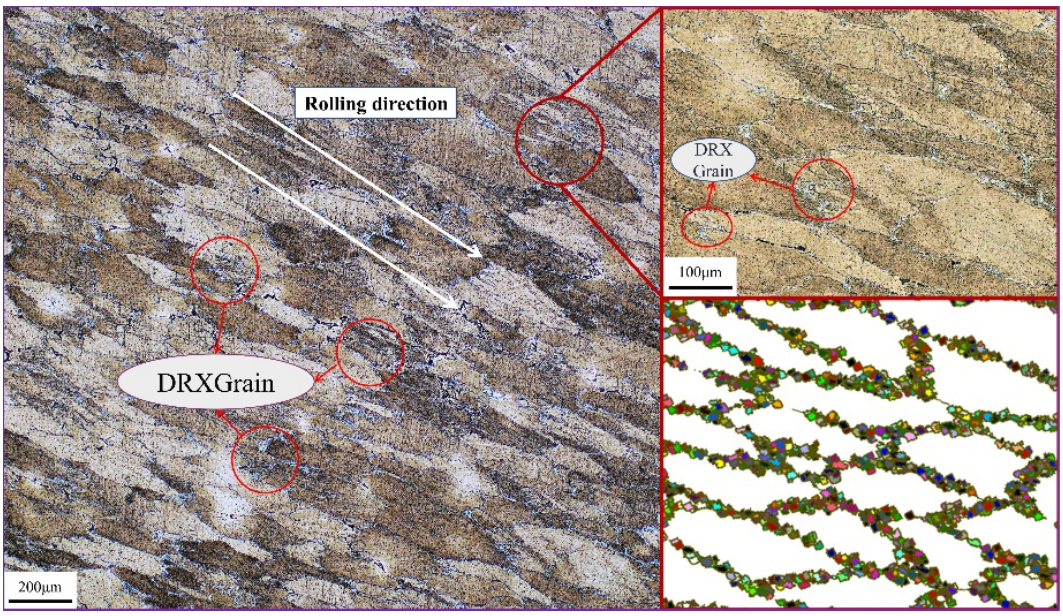


Figure 16. Comparison of the microstructure between the CA simulation and the experimental results.

Further analysis of the experimental results shows that the average grain size of the initial grains is approximately 300 μm, the average grain size after rolling is approximately 250 μm, and the simulation results are approximately 210 μm. The difference is due to the fact that the experimental ring-rolling process is an intermittent deformation process for reference point on the 2219 aluminum alloy ring, with deformation occurring mainly in the deformation zone consisting of the driver and core rollers and in the deformation zone consisting of the conical rollers, which provide energy for recrystallisation nucleation and grain growth. For the reference point in CA simulation, the deformation process is continuous throughout the simulation, under the same strain conditions, resulting in a smaller grain size and a higher degree of recrystallization in the simulation than in the experimental results.

5. Results

1. A model for dynamic recrystallization during ring rolling of large 2219 aluminum alloys was developed to obtain the dynamic recrystallization percentage and the distribution of the average grain size during dynamic recrystallization. The results show that the highest percentage of dynamic recrystallization and the lowest average grain size are found on the outer surface of the aluminum alloy ring and on the intersection of the upper and lower surfaces.
2. A CA model of the microstructure was developed. The dynamic recrystallization that occurs during the rolling process is simulated. Recrystallization nucleation occurs at the grain boundaries, and the recrystallized grains grow and occupy the space of the original grains, resulting in a decrease in overall grain size and grain refinement.
3. The transformation process of the grain shape is studied during the microstructure deformation process. The aluminum alloy is subjected to rolling pressure, and the grains are gradually elongated by the compression deformation, forming bar crystals. Comparing the grain size and morphology of the simulation results with the experimental results, the results show that the CA method is more suitable for visualising the microstructure morphology in a relatively small area, and the finite element method is more suitable for showing the grain size distribution in different areas of the workpiece on a macroscopic scale. Therefore, the combination of the FE subroutine and the CA model provides a more comprehensive understanding of the evolution of the microstructure during the cutting process and its influence on the mechanical behaviour.

Author Contributions: All authors contributed to the study conception. F.H., conceptualization, methodology, software, formal analysis, investigation, writing—original draft; X.M., validation, investigation, writing—review and editing, supervision, project administration, funding acquisition; K.M., validation, investigation, writing—review and editing, supervision. All authors have read and agreed to the published version of the manuscript.

Funding: Tianjin New Material Major Project (18zxclgx0004).

Conflicts of Interest: The authors declare no conflict of interest.

References

1. He, H.; Yi, Y.; Huang, S.; Zhang, Y. An improved process for grain refinement of large 2219 Al alloy rings and its influence on mechanical properties. *J. Mater. Sci. Technol.* **2019**, *35*, 55–63. [CrossRef]
2. Hua, L.; Pan, L.B.; Lan, J. Researches on the ring stiffness condition in radial-axial ring rolling. *J. Mater. Process. Technol.* **2009**, *209*, 2570–2575. [CrossRef]
3. Han, X.H.; Hua, L. Plastic deformation behaviors and mechanical properties of rolled rings of 20CrMnTi alloy in combined radial and axial ring rolling. *Mater. Des.* **2014**, *58*, 508–517. [CrossRef]
4. Sun, Z.C.; Yang, H.; Ou, X.Z. Effects of process parameters on microstructural evolution during hot ring rolling of AISI 5140 steel. *Comput. Mater. Sci.* **2010**, *49*, 134–142.
5. Zhang, H.; Wang, J.; Chen, Q.; Shu, D.; Wang, C.; Chen, G.; Zhao, Z. Study of dynamic recrystallization behavior of T2 copper in hot working conditions by experiments and cellular automaton method. *J. Alloys Compd.* **2019**, *784*, 1071–1083. [CrossRef]
6. Zhang, J.; Li, Z.; Wen, K.; Huang, S.; Li, X.; Yan, H.; Yan, L.; Liu, H.; Zhang, Y.; Xiong, B. Simulation of dynamic recrystallization for an Al-Zn-Mg-Cu alloy using cellular automaton. *Prog. Nat. Sci. Mater.* **2019**, *29*, 477–484. [CrossRef]
7. Xu, W.; Yuan, R.; Wu, H.; Zhong, X.; Guo, B.; Shan, D. Study on the dynamic recrystallization behavior of Ti-55 titanium alloy during hot compression based on Cellular Automaton model method. *Procedia Eng.* **2017**, *207*, 2119–2124. [CrossRef]
8. Hallberg, H.; Wallin, M.; Ristinmaa, M. Simulation of discontinuous dynamic recrystallization in pure Cu using a probabilistic cellular automaton. *Comput. Mater. Sci.* **2010**, *49*, 25–34. [CrossRef]
9. Zhang, Y.; Jiang, S.; Liang, Y.; Hu, L. Simulation of dynamic recrystallization of NiTi shape memory alloy during hot compression deformation based on cellular automaton. *Comput. Mater. Sci.* **2013**, *71*, 124–134. [CrossRef]
10. Qian, M.; Guo, Z. Cellular automata simulation of microstructural evolution during dynamic recrystallization of an HY-100 steel. *Mater. Sci. Eng. A* **2004**, *365*, 180–185. [CrossRef]
11. Chen, F.; Cui, Z.; Liu, J.; Chen, W.; Chen, S. Mesoscale simulation of the high-temperature austenitizing and dynamic recrystallization by coupling a cellular automaton with a topology deformation technique. *Mater. Sci. Eng. A* **2010**, *527*, 5539–5549. [CrossRef]

12. Chen, F.; Qi, K.; Cui, Z.; Lai, X. Modeling the dynamic recrystallization in austenitic stainless steel using cellular automaton method. *Comput. Mater. Sci.* **2014**, *83*, 331–340. [CrossRef]
13. Chen, M.; Yuan, W.; Lin, Y.; Li, H.; Zou, Z. Modeling and simulation of dynamic recrystallization behavior for 42CrMo steel by an extended cellular automaton method. *Vacuum* **2017**, *146*, 142–151. [CrossRef]
14. Sitko, M.; Pietrzyk, M.; Madej, L. Time and length scale issues in numerical modeling of dynamic recrystallization based on the multi-space cellular automata method. *J. Comput. Sci.* **2016**, *16*, 98–113. [CrossRef]
15. Sellars, C.M.; McTegart, W.J. On the mechanism of hot deformation. *Acta Metall.* **1966**, *14*, 1136–1138. [CrossRef]
16. Wen, D.X.; Lin, Y.C.; Zhou, Y. A new dynamic recrystallization kinetics model for a Nb containing Ni-Fe-Cr-base superalloy considering influences of initial δ phase. *Vacuum* **2017**, *141*, 316–327. [CrossRef]
17. Xu, X.; Zhang, J.; Oueriro, J.; Xu, B.; Zhao, W. Multiscale simulation of grain refinement induced by dynamic recrystallization of Ti6Al4V alloy during high speed machining. *J. Mater. Process. Technol.* **2020**, *286*, 116834. [CrossRef]
18. Mecking, H.; Kocks, U.F. Kinetics of flow and strain-hardening. *Acta Metall.* **1981**, *29*, 1865–1875. [CrossRef]
19. Kugler, G.; Turk, R. Modeling the dynamic recrystallization under multi-stage hot deformation. *Acta Mater.* **2004**, *52*, 4659–4668. [CrossRef]
20. Zhou, J.; Mohles, V. Towards realistic molecular dynamics simulations of grain boundary mobility. *Acta Mater.* **2011**, *59*, 5997–6006. [CrossRef]

Disclaimer/Publisher's Note: The statements, opinions and data contained in all publications are solely those of the individual author(s) and contributor(s) and not of MDPI and/or the editor(s). MDPI and/or the editor(s) disclaim responsibility for any injury to people or property resulting from any ideas, methods, instructions or products referred to in the content.